Designing funicular grids with planar quads using i-liwein surfaces

Xavier Tellier, Cyril Douthe, Olivier Baverel, Laurent Hauswirth

Designing funicular grids with planar quads using i-liwein surfaces

Authors: X. Tellier[a*], C. Douthe[a], O. Baverel[a,b], L. Hauswirth[c]

a. Laboratoire Navier, Ecole des Ponts, CNRS, Université Gustave Eiffel, 77455 Champs-sur-Marne, France

b. ENS Architecture, Grenoble, France

c. Laboratoire d'Analyse et de Mathématiques Appliquées, UPEC, CNRS, UGE, Champs-sur-Marne, France

* Corresponding author : xavier.tellier@enpc.fr, +33 1 64 15 37 35

Abstract

The design of curved structural building envelopes is challenging as it requires to account for a wide variety of constraints. In particular, the shape must be mechanically efficient, fabricable, and fit the site geometry. This article shows how a family of surfaces, called *isotropic Linear Weingarten* surfaces (nicknamed i-liwien), may fulfil all these constraints together, and be used as an intuitive design tool. We start by showing that these shapes are funicular for a uniform vertical load, and that principal stress lines form a conjugate net. This allows in particular for the design of gridshells with planar faces and low bending moments or for the design of self-stressed cable nets cladded by planar glass panels. We then propose a discrete model based on recent advances in discrete differential geometry. We use this model to propose a generation method from boundary curves with two additional control parameters. We demonstrate the shape potential on several examples. The application to shells, membranes, cable-nets and gridshells are discussed.

Keywords: Architectural geometry, funicular structures, gridshells, cable-nets, structural design, Monge-Ampère equation, discrete differential geometry

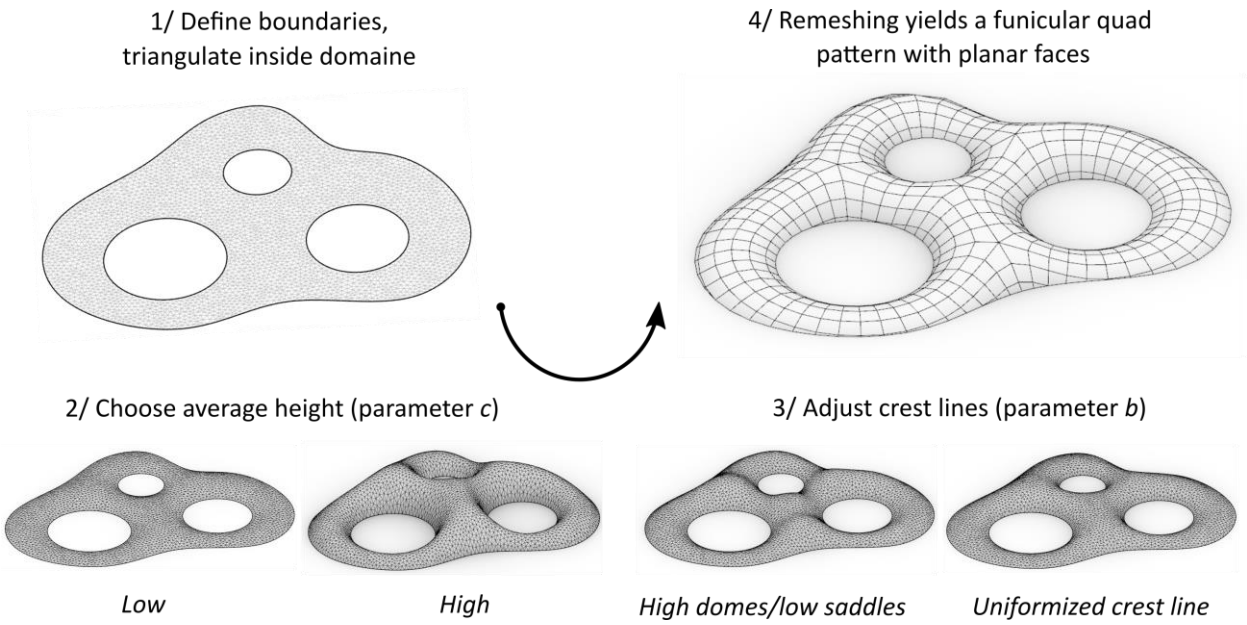

Figure 1: Design workflow for i-liwein surfaces. A designer can control boundary curves and 2 parameters

1 Introduction

Curved structural envelopes combine mechanical efficiency, architectural potential and a wide design space to fulfil functional and environment goals. However, curvature complicates manufacturing, design and assembly, such that cost and construction time are usually significantly higher than for parallelepipedic structures. Furthermore, curvature does not guarantee structural efficiency, but may actually result in the opposite if mechanical considerations are forgotten.

Manufacturing complexity may be reduced by making sure that the structure fulfils geometrical properties specific to the fabrication method. Similarly, mechanical performance may be obtained by structural optimization or form-finding of funicular shapes, which are shapes that can resist a given load with pure axial forces. However, considering the other constraints of a project such as functional requirements and aesthetic, accounting for both fabricability and mechanics leads to highly constrained design problems. In this problem, not only the shape – the surface described by the structure – is important, but also the structural pattern, a term by which we refer to both the orientation and the connectivity of the structural components.

The high complexity of this problem can be a barrier to the use of curved structures on projects, a barrier that happens at two levels for a designer: firstly, what algorithms work and how to use them? Secondly, how to apprehend intuitively the possible shapes?

It is from this perspective that we focus in this article on isotropic Linear Weingarten, that we will nickname i-liwein for brevity, as they happen to have the following properties:

- They offer a rich design space, that contains some popular architectural shapes such as parabolic hyperboloids. The shapes are, we think, smooth and harmonious (see for example Figure 1 and Figure 2).
- They can be covered by a quadrangular pattern with planar faces, such that the edges constitute a funicular beam structure under uniform vertical load - thus combining mechanical performance with a geometrical property which is highly convenient for fabrication of cladding panels. This pattern appears from the so-called isotropic principal curvature lines, and tend to form smooth networks.
- Their behaviour and generation is intuitive and well suited to architectural context: They can be controlled from closed boundary curves, letting then to the designer two degrees of freedom – the first one corresponding to the “inflation” of the shape, the second to the “bumpiness” of its crest line (Figure 1).

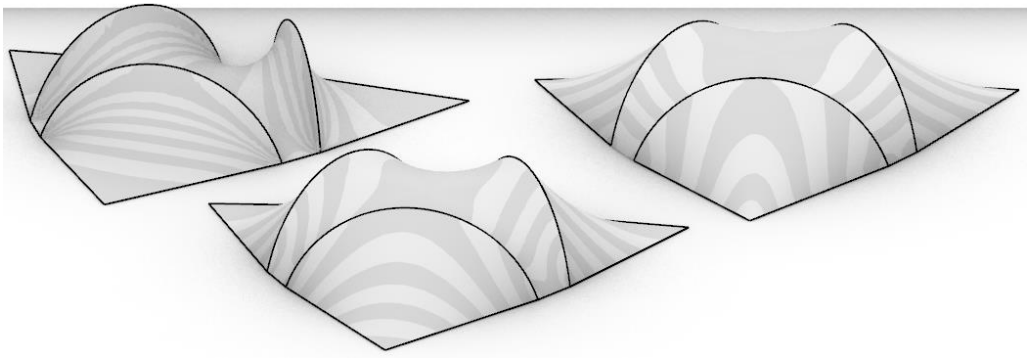

Figure 2: isotropic Linear Weingarten (i-liwein) tensile membranes generated on the same boundary curves (in black)

Overview of paper

After a literature review in subsection 1.1, section 2 presents i-liwein surfaces and the basics of isotropic geometry – the geometrical point of view from which they emerge. In section 3, we show that i-liwein surfaces have an interesting mechanical property: they are funicular under a uniform vertical load, and the principal membrane stress directions then form a conjugate net. This makes them well-suited to design mechanically efficient support structures covered with planar quadrangles.

In section 4, we show how they can be generated on target boundaries. The generation is equivalent to solving a Dirichlet problem of the Monge-Ampere equation. This method allows to control the shape by its boundary curve and by two degrees of freedom. Then, in section 5, we highlight some design applications to membranes (Figure 2), cable-nets (Figure 3), gridshells

(Figure 1) and funicular shells. Section 6 presents two case studies that investigate the mechanical performance of i-liwein shells for various values of the parameter *b,* considering in particular non-uniform loads. We finish in section 7 by a discussion of design applications and performances.

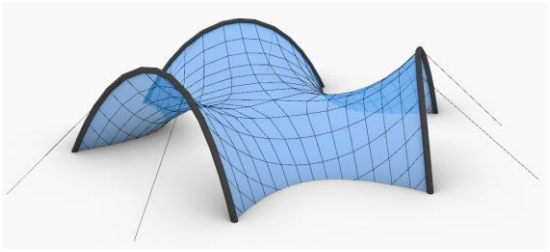

Figure 3: A self-stressed cable-net with planar quad glass panels supported at cable crossings

1.1 Previous work

Before getting started on i-liwein surfaces, we will be reviewing here the design methods for double-curvature structures that account for both mechanical efficiency and fabricability. We subdivide the literature based on how the topology and shape are dealt with, as this is the main difference of our approach with the core of the literature on the topic.

From topology to shape

Many design methods take topology as an input, and explore the possible shapes. For example, hanging models, which have been used abundantly for shell and membrane design by master-builders such as Heinz Isler, Frei Otto or Antonio Gaudi, give funicular shapes that correspond to a specific net configuration. Using a hanging cable net with constant edge length gives a shape that is both funicular and realizable as an elastic gridshell – a strategy used to find the form of the Mannheim gridshell (*Happold and Liddel* 1975). The numerical form-finding methods, such as force density *(Schek 1974),* particle-spring method, or the thrust network analysis TNA (Block 2009), also take pattern as an input. The orientation and connectivity of the starting pattern may change drastically the shape resulting from these methods, as highlighted in (Ramm and Wall 2004). Similarly, orientation and connectivity are key parameters when optimizing a geometry to combine mechanical efficiency and fabrication properties such as face planarity, as is for example done in (Adriaenssens et al. 2012), (Feng and Ge 2013), (Mesnil et al. 2018) or (Tang et al. 2014).

From shape to topology

Another common design approach is to take a shape as an input, and to find an optimal pattern on it. For structural performance, optimal pattern for a quad gridshell or a waffle shell is commonly searched by aligning the pattern with principal stress nets. Similarly, considering

fabrication alone is done by aligning the pattern with specific surface curves or parametrizations, such as conjugate nets (Vouga et al. 2012; Zadravec, Schiftner, and Wallner 2010), geodesics, asymptotic curves (Schling, Hitrec, and Barthel 2017), conformal patterns or principal curvature lines (Bo et al. 2011; Tellier et al. 2019b; Wang and Liu 2009).

Structural performance and fabricability can also be searched together with this approach. For example, (Schiftner and Balzer 2010) propose to pattern a surface following maximum stress lines and their conjugate directions. (Oval 2019; Oval et al. 2018) propose a method to explore various topologies and compare their performances.

From boundaries to shape and topology

The two above approaches may be limited when trying to obtain too many properties from the geometry at the same time. For example, (Sun 2016) studied how to design a surface fitting a target boundaries in which principal stress lines coincide with principal curvature lines in a "topology to shape" approach. The limited success of this approach led the team to relax entirely the topology: in (Pellis and Pottmann 2018), the alignment of principal stresses and curvature is obtained by a new constraint on triangular meshes. The topology of the structural pattern is not imposed beforehand; it instead appears in a subsequent remeshing step.

This article will use the same approach: given our mechanical and fabrication constraints (funicularity and face planarity), we derive both the optimal topology and the optimal shape from the boundaries. This is permitted by *a formulation of these properties which is independent of surface parametrization*.

This article extend the work presented at the AAG2020 conference in the continuation of the work presented in (Tellier et al. 2018, 2019a, 2020, 2021), in which we looked at the generation of constant mean curvature and Linear Weingarten surfaces (not isotropic): on these surfaces, principal stresses and curvature are aligned under a uniform normal pressure load. The present work differs in the sense that we will now consider vertical uniform loads, which model better self-weight and snow loads.

2 i-liwein surfaces

2.1 Isotropic geometry

Isotropic Linear Weingarten surfaces (i-liwein) are objects of *isotropic geometry*. Isotropic geometry is a way to describe the geometry of shapes with a specific set of tools, in which the vertical direction plays a particular role. A thorough treatment can be found in (Sachs 1990). (Pottmann and Liu 2007) gives a concise introduction.

In isotropic geometry, the notions of distance, angles and curvature differ from the traditional Euclidian geometry. They are all computed relatively to a vertical projection on the horizontal plane. The notion of surface curvature is also described differently. This difference is best understood by looking at a planar curve $z = f(x)$ (Figure 4). There are two ways to describe the inclination of the tangent of such a curve:

- The angle it makes with a reference axis (e.g. a horizontal axis);
- The slope dz/dx.

With the first one (the angle), the curvature is naturally understood as the variation of the angle of the tangent as we move along the curve ($d\alpha/ds$, with $ds = \sqrt{dx^2 + dz^2}$), which is the inverse of the radius of the tangent circle: this is the Euclidian curvature. With the second one (the slope), the curvature is best defined as the variation of slope with respect to x (d^2z/dx^2): this is the isotropic curvature.

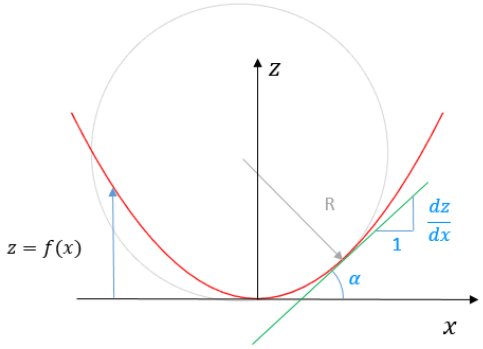

	Euclidian geometry	Isotropic geometry
Inclination	α	$\frac{dz}{dx}$
Curvature	$k = \frac{d\alpha}{ds} = \frac{1}{R}$	$k^i = \frac{d^2z}{dx^2}$

Figure 4: Description of curvature in Euclidian and isotropic geometry

We remark that the slope of a vertical line is infinite: isotropic geometry is not the right tool to describe curves with vertical tangents or surfaces with vertical tangent planes. It is then natural to describe surfaces as height fields:

$$(x, y) \mapsto (x, y, f(x, y)) \qquad (1)$$

We will mostly use this way of parametrizing surfaces throughout this paper. The role of the curvature tensor is played by the hessian of f:

$$\nabla^2 f = \begin{bmatrix} \partial_{xx} f & \partial_{xy} f \\ \partial_{xy} f & \partial_{yy} f \end{bmatrix}$$

$\nabla^2 f$ is symmetric, so it admits two orthogonal eigenvectors in the xy plane, which are called the *i-principal directions*. The maximum and minimum eigenvalues, $f_1$and f_2, are called *i-principal curvatures*. By integrating the i-principal directions, one obtains the i-principal curvature lines. They differ from the Euclidian principal curvature lines. However, they still form a conjugate net,

which is a smooth equivalent of planar quad meshes (Sauer 1970). Furthermore, their vertical projection on the xy plane is an orthogonal net.

2.2 i-liwein surfaces

Similarly, to Euclidian geometry, the Gauss and mean curvature can be defined as the determinant and half-trace of the curvature tensor (an *i* superscript is used to differentiate them from the traditional Euclidian curvatures):

$$K^i = \partial_{xx} f \partial_{yy} f - \partial_{xy} f^2 = f_1 f_2$$

$$H^i = \frac{1}{2}\left(\partial_{xx} f + \partial_{yy} f\right) = \frac{1}{2}\Delta f = \frac{1}{2}(f_1 + f_2)$$

i-liwein can then be defined as the surfaces verifying at each point:

$$aH^i + bK^i = c \qquad (2)$$

for given constant real coefficients *a, b* and *c*.

2.3 Examples

It turns out that some well-known families of surfaces satisfy equation (2), including popular shapes in architecture.

2.3.1 Paraboloids

Paraboloids are a very common family of shapes for shells (see Figure 5). With a proper choice of axes and origin, their equation reads:

$$z = \alpha x^2 + \beta y^2$$

If $\alpha\beta < 0$, the surface is called a hyperbolic paraboloid (or « hypar »), and contains two families of straight lines. If $\alpha\beta > 0$, the surface is called an elliptic paraboloid. The Hessian of the height field reads:

$$\nabla^2 f = \begin{bmatrix} 2\alpha & 0 \\ 0 & 2\beta \end{bmatrix}$$

Paraboloids are isotropic LW surfaces, as their mean and Gaussian curvature are both constant:

$$H^i = \alpha + \beta$$

$$K^i = 4\alpha\beta$$

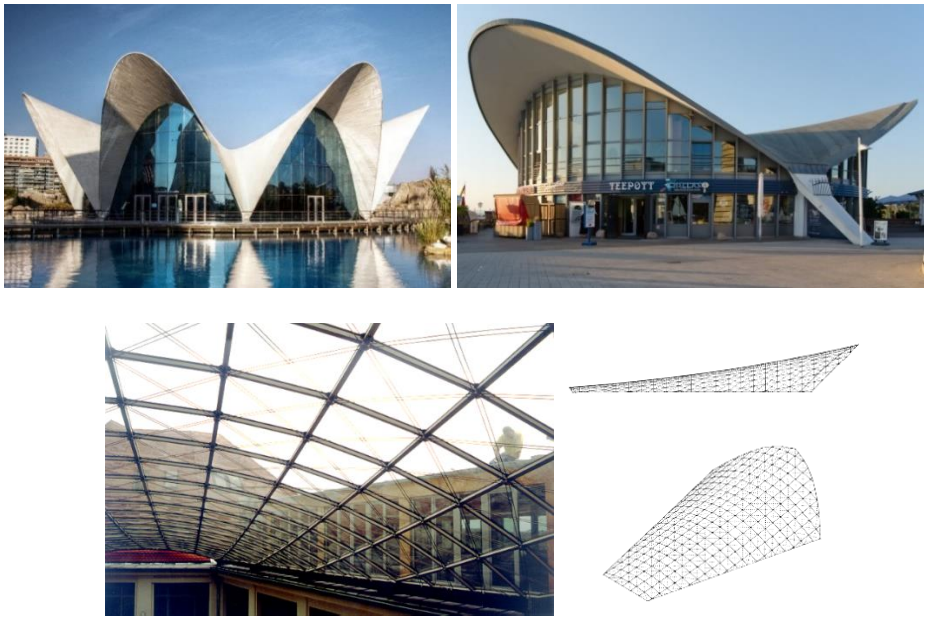

Figure 5: These three structure are composed of paraboloids, which are a special types of isotropic LW surfaces.

Top left: El Oceanográfico (F. Candela), Valencia, Spain (©Felipe Gabaldón);

Top right: Teepott restaurant, Warnemünde, Germany (©An-D) ;

Bottom: Courtyard roof Industriepalast, Leipzig (reproduced with permission from (Glymph et al. 2004))

There is actually one degree of freedom to define the (a, b, c) coefficients of the LW relationship (more precisely, one more degree of freedom than the trivial scaling of *a, b* and *c*). If we fix the trivial scaling of (a, b, c) by setting either $c = 0$ or $c = 1$, equation (1) is verified for any value of a as long as:

$$b = \frac{\mathrm{c} - a(\alpha + \beta)}{4\alpha\beta} \qquad (3)$$

2.3.2 Pelikan surfaces

Membranes for which the membrane stress tensor, when projected in the horizontal plane, is constant, are called *Pelikan surfaces*. They were introduced in (Pelikan 1958). These surfaces have been generated by dynamic relaxation (Hincz and Gaspar 1999), and have been used for example to design of membranes and concrete shells, such as the Keramion ceramics museum in Frechen (Figure 6), for which a tensile membrane was used as a formwork for a concrete shell (www.keramion.de).

Figure 6: The concrete shell of the Keramion museum in Frechen, Germany, is a Pelikan surface – a special type of i-LW surface also referred to as i-minimal. ©Klaas Vermaas

2.3.3 Harmonic functions as height fields

Scalar harmonic functions of the plane are functions for which the Laplacian is null at any point: $\Delta f = 0$. They are therefore field heights of i-minimal surfaces, i.e. surfaces verifying $H^i = 0$. There is a rich mathematical theory behind these surfaces. One method to generate a rich variety of analytical harmonic functions is via complex holomorphic functions (Cartan 1963). A holomorphic function of a region $D \subset \mathbb{C}$ is a function $f: D \to \mathbb{C}$ which is conform, i.e. it transforms an infinitesimal square into another infinitesimal square. Most of the complex functions that one could think about that do not contain the complex conjugate $\bar{z}$ are holomorphic. This is the case in particular of the following functions:

- Polynomials. Ex : $f(z) = z^7 - 42iz \ , z \in \mathbb{C}$
- Rational functions (fractions of polynomials). Ex : $f(z) = \frac{z+1}{z-1}$
- Exponential functions. Ex : $f(z) = \frac{e^{iz}+e^{-iz}}{2} = \cos z$
- Linear combination of harmonic functions. Ex : $f(z) = e^z + 1/z$

The link with i-minimal surfaces appears with an important theorem about holomorphic functions: Their real part and imaginary part are both harmonic. Figure 7 shows several i-minimal surfaces generated using this property:

- Top left: $f(z) = Re(\log z)$ where $Re(z)$ is the real part of a complex number z.
- Top middle: Monkey saddle of order 3: $f(z) = Re(z^3) = x^3 - 3xy^2$
- Top right: $f(z) = Re(1/\|z\|^2)$
- Bottom left: $f(x, y) = \cos x \exp(y - 1) + \cos(x + \pi) \exp(-y - 1)$
- Bottom right: $f(z) = Re(\tan^{-1}(z))$

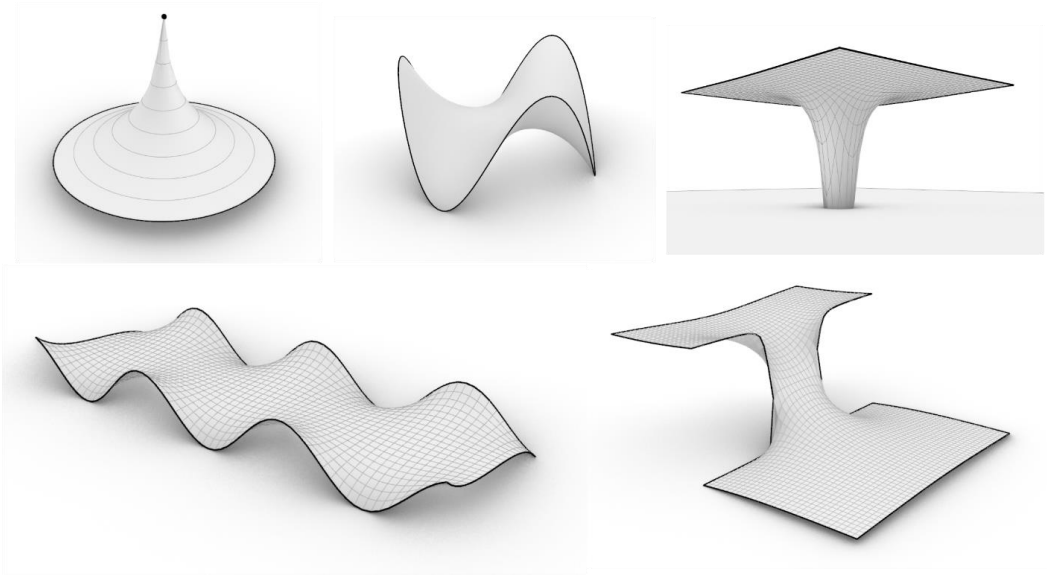

Figure 7: Analytical i-minimal surfaces – each surface can be realized as a tension membrane

2.3.4 Developable surfaces

Developable surfaces are characterized by $K = 0$. For a height field surface defined as in equation (1), K and K^i are related by (do Carmo 1976):

$$K = \frac{\partial_{xx} f \partial_{yy} f - \partial_{xy} f^2}{\left(1 + \partial_x f^2 + \partial_y f^2\right)^2} = \frac{K^i}{(1 + \|\nabla f\|^2)^2}$$

Therefore, any developable surface ($K = 0$) that can be described as a height field is i-liwein ($K^i = 0$).

Note:

The mean curvature can also be expressed as a function of the isotropic mean curvature:

$$H = \frac{H^i + \frac{1}{2}\,\nabla f . \widehat{\nabla^2 f} . \nabla f}{(1 + \|\nabla f\|^2)^{3/2}}$$

From that expression, it appears clearly that there is no equivalence between minimal and i-minimal.

2.3.5 Surfaces of revolution and helices

(Ogrenmis 2016) solved the ordinary differential equation fulfilled by the meridian of an i-liwein surface of revolution, and gives the analytical solution. There are two degrees of freedom to design the meridian for a given set of coefficients (a, b, c) – except for some degenerate coefficients for which there is only one. (Yoon and Lee 2016) performed the same work for i-liwein surfaces with helicoidal symmetry.

3 Mechanics of i-liwein surfaces

3.1 Funicularity

This section shows that i-liwein surfaces enjoy a mechanical property very similar to their Euclidian counterparts. This property is best expressed using the tensor $\mathbf{N^i}$ of projected membrane stresses in the xy plane.

Proposition 1

Let us consider a shell with membrane-compatible support conditions and with an i-liwein reference surface fulfilling equation (2) (a$H^i + bK^i = c$).

If $c \neq 0$, the shell is funicular for uniform vertical loads we_z (w is in kN/m^2). The projected membrane stresses are given by:

$$\mathbf{N^i} = \frac{w}{2c}\left(a\,\mathbf{I} + b\,\widehat{\nabla^2 f}\right)$$

Where $\mathbf{I}$ the identity tensor of the xy plane, and $\widehat{\nabla^2 f}$ is the tensor obtained by rotating the hessian $\nabla^2 f$ by +90° around the z axis:

$$\widehat{\nabla^2 f} = \begin{bmatrix} \partial_{yy} f & -\partial_{xy} f \\ -\partial_{xy} f & \partial_{xx} f \end{bmatrix}$$

If $c = 0$, the shell admits a one parameter family of self-stress fields given by:

$$\mathbf{N^i} = \lambda\left(a\,\mathbf{I} + b\widehat{\nabla^2 f}\right)\ ,\lambda \in \mathbb{R}$$

Corollary

Under a uniform vertical load, principal membrane stresses on an i-liwein shell form a conjugate net and coincide with i-curvature directions. Discretization by stress lines hence give quadrangles which are near-planar.

Proof:

Membrane equations can be written in Cartesian coordinates, as detailed for example in (Ventsel and Krauthammer 2001). The projected membrane stress field $\mathbf{N^i}$ is at equilibrium under a vertical load Ge_z if it verifies:

$$div\ \mathbf{N^i} = \mathbf{0}$$

$$div(\mathbf{N^i}.\nabla f) = G$$

These equations correspond respectively to the horizontal and vertical equilibrium. The fact that $div\ \mathbf{N^i} = 0$ can be used to simplify the vertical equilibrium equation in the form:

$$tr(\mathbf{N^i}.\nabla^2 f) = G$$

The divergence of the stress fields from the proposition are:

$$div\ \mathbf{N^i} = \frac{w}{2c}\left(a\ div\ \mathbf{I} + b\ div(\widehat{\nabla^2 f})\right)$$

Obviously, $div\ \mathbf{I} = 0$. Furthermore, by expressing $\widehat{\nabla^2 f}$ in x, y coordinates:

$$div\left(\widehat{\nabla^2 f}\right) = div\begin{bmatrix} \partial_{yy} f & -\partial_{xy} f \\ -\partial_{xy} f & \partial_{xx} f \end{bmatrix} = 0$$

The proposed stress fields are therefore at horizontal equilibrium.

The vertical equilibrium is obtained by expressing $\nabla^2 f$ and $\widehat{\nabla^2 f}$ in the i-principal curvature directions:

If $c \neq 0$:

$$tr(\mathbf{N^i}.\nabla^2 f) = \frac{w}{2c} tr\left(\left(a\begin{bmatrix}1 & 0\\ 0 & 1\end{bmatrix} + b\begin{bmatrix}f_2 & 0\\ 0 & f_1\end{bmatrix}\right)\begin{bmatrix}f_1 & 0\\ 0 & f_2\end{bmatrix}\right)$$

$$= \frac{w}{2c}(a(f_1 + f_2) + 2bf_1 f_2)$$

$$= \frac{w}{2c}\left(2aH^i + 2bK^i\right)$$

$$= w$$

The same reasoning applies to the case $c = 0$. The corollary stems from the fact that eigenvectors of $\nabla^2 f$ are also eigenvectors of $\widehat{\nabla^2 f}$, which in turn are eigenvectors of $a\ \mathbf{I} + b\widehat{\nabla^2 f}$.

The corollary is proved by remarking that the eigenvectors of $\mathbf{N^i} = \lambda\left(a\ \mathbf{I} + b\widehat{\nabla^2 f}\right)$ are the eigenvectors of $\widehat{\nabla^2 f}$:

$$with\ k \in \mathbb{R}, \lambda\left(a\ \mathbf{I} + b\widehat{\nabla^2 f}\right)\boldsymbol{u} = k\boldsymbol{u} \iff \widehat{\nabla^2 f}\boldsymbol{u} = \left(\frac{k/\lambda - a}{b}\right)\boldsymbol{u}$$

Since $\nabla^2 f$ is symmetric, its eigenvectors are orthogonal. As $\widehat{\nabla^2 f}$ is obtained by rotating $\nabla^2 f$ in-plane by 90°, eigenvectors of $\widehat{\nabla^2 f}$ and $\nabla^2 f$ coincide. We can conclude that the eigendirections of $\mathbf{N^i}$ coincide with i-principal curvature directions of the surface f. ■

3.2 Link with Airy stress function

Planar stress tensors at equilibrium without external loads can be expressed with the hessian of a scalar function Φ, called the Airy stress function. When a shell is subject to purely vertical forces, such a function can be used to describe the projected stress tensor $\boldsymbol{N^i}$:

$$\boldsymbol{N^i} = \widehat{\nabla^2 \Phi}$$

In our case, the Airy stress function Φ is :

$$\Phi(\mathrm{x}, \mathrm{y}) = \frac{a}{2}(x^2 + y^2) + bf(x, y)$$

The Airy stress function is hence a linear combination of the heights of the isotropic sphere and of the surface height itself, which is a remarkable property.

3.3 Application to paraboloids

The above result can be applied to paraboloids with an interesting consequence: they are funicular for two different load cases. Given a paraboloid $z = \alpha x^2 + \beta y^2$ we have two possible choices for parameter c, $c = 0$ or $c = 1$:

With $c = 1$, we can interpret the shape as funicular under uniform vertical. Using equation (3), there is a one-parameter family of admissible stress fields :

$$\mathbf{N^i} = \frac{w}{2}\left(a\, I + b\, \widehat{\nabla^2 f}\right) = \frac{w}{2}\left(a \begin{bmatrix}1 & 0\\ 0 & 1\end{bmatrix} + \left(\frac{1 - a(\alpha+\beta)}{4\alpha\beta}\right)\begin{bmatrix}2\beta & 0\\ 0 & 2\alpha\end{bmatrix}\right), a \in \mathbb{R}$$

With $c = 0$, we find another family of admissible stress fields, which corresponds to self-stressed states:

$$\boldsymbol{N^i} = a\, \boldsymbol{I} + b\widehat{\nabla^2 f} = a\left(\begin{bmatrix}1 & 0\\ 0 & 1\end{bmatrix} - \frac{(\alpha+\beta)}{2\alpha\beta}\begin{bmatrix}\beta & 0\\ 0 & \alpha\end{bmatrix}\right), a \in \mathbb{R}$$

The fact that paraboloids are at the same time self-stress shapes and funicular shaped under uniform load is remarkable. For example, if a hypar membrane or cable-net (case $\alpha\beta < 0$) is used as a formwork for casting a concrete shell, the membrane deflection under the dead load of the fresh concrete is expected to be very low compared to other arbitrary membrane shapes: deflections will be mostly due to material stretching rather than to a deflection to get into a funicular shape. We remark that if $\alpha + \beta = H^i \neq 0$, warp and weft of the membranes need to be aligned with the horizontal x and y axes – otherwise the stress field is not admissible.

Patching paraboloids

Rows of paraboloids can be assembled to form a C^1 surface that is still i-liwein. Indeed, let us consider the paraboloids of Figure 8 which form a row on the x axis. Blue and white patches can be described respectively by equations $z = \alpha_{blue}x^2 + \beta y^2$ and $z = \alpha_{white}x^2 + \beta y^2$, β being identical to insure continuity. If we set:

$$a = 1\,;\, b = \frac{-1}{4\beta}\,;\, c = \beta$$

Then, for both blue patches:

$$aH^i + bK^i = (\alpha_{blue} + \beta) + \frac{-1}{4\beta}\, 4\alpha_{blue}\beta = \beta = c$$

The same results hold for the white patches. The surface is therefore i-liwein. The fact that it is not C^2 does not alter the mechanical properties: we can find a continuous membrane stress field across the whole surface under uniform vertical load. It does not either alter the panelling by planar quads, because the i-principal curvatures are aligned with the x and y axes for all patches.

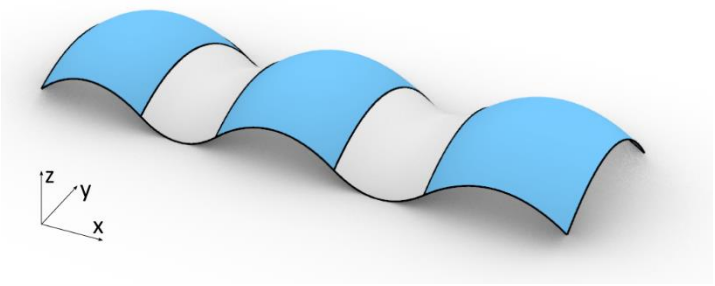

Figure 8: C^1 i-liwein surface composed of paraboloids

This reasoning can be actually extended to an arbitrary number of patches $z = \alpha_i x^2 + \beta y^2, i = 1,2 \dots, n$, or even to a translation surface generated by translating a parabola of the yz plane along a curve of the xz plane, i.e. a surface with equation:

$$z = g(x) + \beta y^2$$

where g is an arbitrary real continuous function and β a real number.

3.4 Invariance by x, y or z scaling

One can easily prove that the vertical scaling conserve the i-liwein property. However, a horizontal scaling (for example a 1D-scaling of x direction) transforms equation (2) into the form:

$$a_x \partial_{xx} f + a_y \partial_{yy} f + b_0 K^i = c_0$$

The same reasoning as in 3.1 shows that these surfaces are also funicular under a uniform vertical load. In particular, scaling an i-CMC surface ($H^i = cte$) yields surfaces with constant projected stress tensors, i.e. a general Pelikan surfaces.

3.5 Extension to surfaces funicular to self-weight

Proposition 1 considers a uniform vertical load. This is often a good approximation of dead load if the slope of an envelope is small, and it is always a good model of symmetric snow loads. However, in shell structure of constant thickness with high slopes, this approximation might not be precise. The result of proposition 1 can actually be adapted for this setting to search for surfaces with constant projected stresses:

Proposition 2

A shell of constant thickness with reference surface $z = f(x, y)$ such that:

$$\frac{tr(\nabla^2 f)}{\sqrt{1 + \|\nabla f\|^2}} = c \ , c \in \mathbb{R}$$

is self-supported: It can resist its own weight with pure membrane stresses, such that the projected membrane stress tensor in the horizontal plane is isotropic and constant.

Proof:

Self-weight is a vertical load of amplitude:

$$G(x,y) = \mu \sqrt{1 + \|\nabla \mathrm{f}\|^2} \ , \mu \in \mathbb{R}$$

Where G is expressed for example in kN per m² of projected area in the *xy* plane. Let us consider the projected stress tensor $\mathbf{N^i} = \frac{\mu}{c}\ \mathbf{I}$. It verifies $div\ \mathbf{N^i} = \mathbf{0}$. Furthermore:

$$tr(\mathbf{N^i}.\nabla^2 f) = tr\left(\frac{\mu}{c}\ \nabla^2 f\right) = \mu \sqrt{1 + \|\nabla \mathrm{f}\|^2} = G$$

$\mathbf{N^i}$ is therefore at equilibirum under the load G. ■

This equation opens the way to the search of analytical self-supporting grids. One could for example search for a family of funicular surfaces of revolution: Their meridians could be found by solving an ordinary differential equation, with one variable. One could also look for funicular surfaces of translations. These surfaces will not be addressed further in this article.

3.6 Recovering membrane stresses

The membrane stress tensor $\mathbf{N}$ can be recovered from the projected tensor $\mathbf{N^i}$ following equations given for example in (Frey and Studer 2003). Let us call:

- $\boldsymbol{e_x}$ and $\boldsymbol{e_y}$ the base vectors of the plane xy;
- $\boldsymbol{e_x^S}$ and $\boldsymbol{e_y^S}$ the projections of the base vectors $\boldsymbol{e_x}$ and $\boldsymbol{e_y}$ in the tangent plane of the surface. These vectors are in general not orthogonal;
- N_{xx}, N_{xy}, N_{yy}, the components of the membrane tensor $\mathbf{N}$ in the basis $(\boldsymbol{e_x^S}, \boldsymbol{e_y^S})$. $N_{xx}\ \boldsymbol{e_x^S} + N_{xy}\ \boldsymbol{e_y^S}$ (respectively $N_{xy}\ \boldsymbol{e_x^S} + N_{yy}\ \boldsymbol{e_y^S}$) is then the membrane stress vectors acting on a facet with normal $\boldsymbol{e_x^S}$ (resp. $\boldsymbol{e_y^S}$);
- α and β are the slope angles in the x and y directions:

$$\tan\alpha = \partial_x f \ ; \ \tan\beta = \partial_y f$$

The coefficients of the membrane stress tensor are then:

$$N_{xx} = N^i_{xx}\frac{\cos\beta}{\cos\alpha} \ ; \ N_{xy} = N^i_{xy} \ ; \ N_{yy} = N^i_{yy}\frac{\cos\alpha}{\cos\beta}$$

Note: Despite the fact that $N_{xy} = N^i_{xy}$, principal directions of $\mathbf{N^i}$ (for which shear is null) are not the projections of the principal directions of $\mathbf{N}$. This is due to the fact that the x and y axes do not project in general to orthogonal axes on the membrane tangent plane.

4 Generation of i-LW surfaces from boundary curves

In this section, a generation method for elliptical i-liwein surfaces (verifying $a^2 + 4bc > 0$) from a boundary curves is presented.

4.1 The Monge-Ampere equation

As i-liwein surfaces are necessarily height fields, they can be generated by solving the partial differential equation (2) in a function f of z. This is a special case of the Monge-Ampère equation as it can be written in the form (Courant and Hilbert 1962):

$$E\left(\partial_{xx}f\,\partial_{yy}f - \partial_{xy}f^2\right) + A\,\partial_{xx}f + 2B\,\partial_{xy}f + C\,\partial_{yy}f + D = g(x,y)$$

With $E = b$; $A = C = \frac{a}{2}$; $B = 0$; $D = -c$; $g(x,y) = 0$

The Monge Ampere equation has many physical applications, ranging from optimal transport problems (Benamou, Froese, and Oberman 2014; Villani 2003) to reflector design (Wu et al. 2013). It also has many applications in differential geometry, allowing for example the proof of the existence of particular types of surface (Trudinger and Wang 2008). Numerical resolution has been addressed quite recently by research. A review of is given in (Neilan, Salgado, and Zhang 2020).

This problem is particularly complex to solve for the following reasons:

- It is a fully nonlinear problem: the term with highest derivative is not linear;
- Solutions have low regularity and are not unique;
- Weak solutions are not based on variational principles. A significant portion of the literature is devoted to viscosity solutions, which may have weaker regularity;
- Existence and uniqueness of solutions is subject to a constraint on the convexity of the solution and domain – which is a strong constraint for application to architecture.

Many resolution methods are based on finite differences and a quad grid discretization of the plane, (Benamou, Froese, and Oberman 2010; Dean and Glowinski 2003, 2004; Oberman 2008). These are less suited for irregular contours, as are likely to occur in an architectural context. Also, these methods only search for a convex solution to the problem, which we will refer to as *type II*, in section 4.3.1.

(Feng and Jensen 2017) introduced a finite-element formulation based on a triangular discretization. It was used in (Jensen 2018) to explore some solutions of the Monge-Ampere equation on non-convex domains. As this method is relatively complex, we will use the fact that, in our context, $g = cte$, to propose a simpler generation method based on a quadratic discrete operator on triangular meshes from discrete differential geometry.

4.2 Discrete i-liwein surfaces

Discrete curvature models

We discretize i-liwein surfaces by using the vertex-wise discrete model for H^i and K^i for unstructured triangular meshes proposed in (Pottmann and Liu 2007). The calculation steps to compute the curvature of a vertex v in a mesh *M* are the following:

i. Compute the metric dual of the planes of the faces adjacent to vertex v. The dual of the plane of a face i is a point, which, once projected vertically onto the xy plane, yields a point m_i. The points m_i form a closed polygon L_m. The area of this polygon, $A(L_m)$ can be calculated as:

$$A(L_m) = \frac{1}{2}\sum \det(m_i, m_{i+1})$$

ii. Project the 1-star of v vertically on the Maxwell paraboloid Σ. Compute the metric dual of the projected faces: they form a closed polygon. Project it onto the xy plane, thus forming the polygon $s_1 s_2$ … called L_s, with oriented area A(L_s).

iii. Compute the mixed area of polygons L_M and L_S, defined as:

$$A(L_M, L_S) = \frac{1}{4}\sum (\det(m_i, s_{i+1}) + \det(s_i, m_{i+1}))$$

iv. The discrete Gaussian and mean curvature are then computed as:

$$K^i(v) = \frac{A(L_m)}{A(L_s)}, \quad H^i(v) = \frac{A(L_m, L_s)}{A(L_s)}$$

Notes:

- With this model, vertices should not have too high x or y coordinates: The projection to the i-sphere gets points to an altitude $x^2 + y^2$, working tolerance can be reached easily.
- $H^i(v)$ could be calculated in a more simple way by taking a discrete Laplacian of the z coordinates of the vertices. The chosen discretization is more complex, but more consistent with the discrete model of K^i.

Assessment of discrete model

Figure 9 shows the values given by these two discrete models for two triangular meshes inscribed in paraboloids – for which the Gaussian and mean curvature are known analytically. By *inscribed*, we mean that the mesh vertices are exactly on the surfaces. We observe that the discrete curvatures are very close to the ones of the smooth paraboloids for the synclastic paraboloid. However, high discrepancies are observed for K^i for the hypar, especially for nodes of valence different from 6, and in areas of high slope. This problem of approximation of Gaussian curvature for inscribed meshes was identified in (Borrelli, Cazals, and Morvan 2003) in Euclidian geometry. We observe the same issue in isotropic geometry. However, we shall see in section 4.5 that these discrepancies are not an issue in our method because they are due to the fact that we use inscribed meshes.

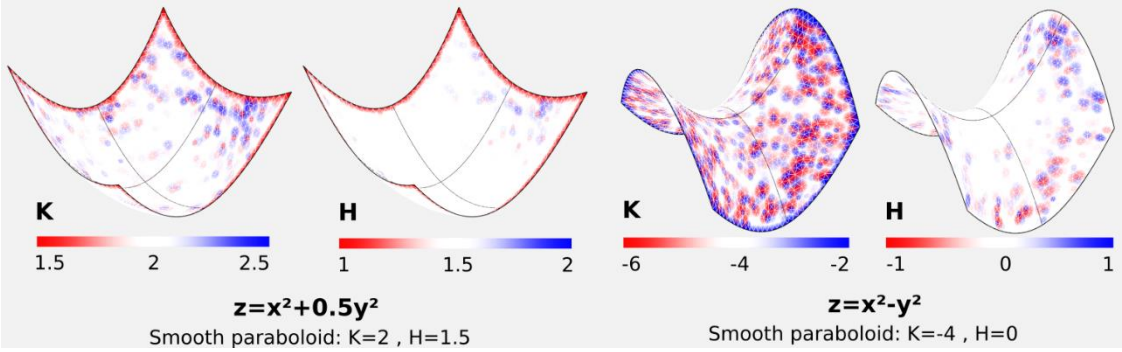

Figure 9: Evaluation of discrete models for isotropic Gaussian and mean curvatures

i-liwein meshes

From these discrete models, *i-liwein triangular meshes* can naturally be defined as meshes for which a linear combination of these two curvatures is constant for each vertex:

$$\forall\ vertex\ v, \qquad aH^i(v) + bK^i(v) = c, \qquad a, b, c \in \mathbb{R}$$

4.3 Preliminaries on smooth i-liwein surfaces

4.3.1 Type I and II solutions

Important geometrical insight on i-liwein surfaces can be obtained from the curvature diagram, i.e. a diagram plotting the value of H^i and K^i at each surface point (Figure 10). For i-liwein surfaces, this diagram is included in a straight line. We observe that the isotropic Gaussian and mean curvature verify the inequality:

$$H^{i\,2} - K^i = \left(\frac{f_1 - f_2}{2}\right)^2 \geq 0$$

There is hence a domain of the diagram which is impossible geometrically (in red). If $a^2 + 4bc \geq 0$, the line defined by equation (2) crosses this forbidden domain. The curvature diagram is hence included in the union of two rays (semi-infinite lines). Now, in a smooth surface, curvatures vary continuously: the curvature diagram is a one-connected domain. As a result, the curvature diagram of an i-liwein surface with $a^2 + 4bc \geq 0$ cannot be on both rays. We will call type I (resp. type II) the i-liwein surfaces having their curvature diagram entirely in the left (resp. right) ray. From a design perspective, type I surfaces are more interesting formally than type II, because the latter tend to look quite spherical.

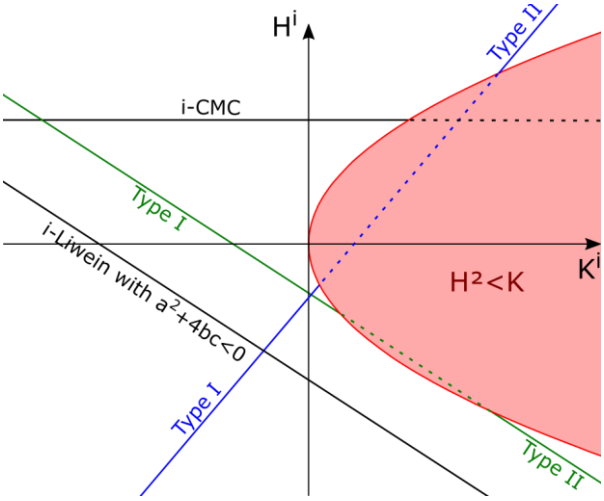

Figure 10: Curvature diagram

4.3.2 Condition for elliptic PDE

One can show that, if $b \neq 0$, equation (2) can be put in the following form with the change of variable

$g(x,y) = f(x,y) + \frac{a}{4b}(x^2 + y^2)$:

$$4b^2 K^i(g) = a^2 + 4bc$$

Solving equation (2) with $a^2 + 4bc > 0$ is therefore equivalent to computing the geometry of a surface with positive constant i-Gaussian curvature. This problem is elliptic, and is hence well suited to a generation from a closed boundary.

4.4 Generation method

We introduce an iterative method to solve the equation, with the following simple pseudo-code:

i. Triangulate domain

ii. Create initial solution (e.g. z=0 or minimal)

iii. Iterate the following steps until displacements are below tolerance:

   a. Solve the equation $aH^i + bK^i = c$ for each vertex individually, assuming that neighbours are fixed.

   b. Move each vertex to the calculated position.

Local resolution

The key step of the algorithm is the resolution with fixed neighbours (step iii.a). The equation is nonlinear, but we remark that, as the centre vertex of a 1-star is moved along a vertical axis:

- $A(L_s)$ does not change;
- $A(L_m)$ varies quadratically;
- $A(L_m, L_s)$ varies linearly.

Hence, H^i and K^i vary respectively linearly and quadratically with a vertex height. Therefore, $aH^i + BK^i - c$ is quadratic in z. Thus, there exists real coefficients α, β and γ such that:

$$aH^i + bK^i - c = P(z) = \alpha z^2 + \beta z + \gamma$$

The resolution in z is then straightforward, we use the following method:

Case $b = 0$

If $b = 0$, the equation is linear. This case corresponds to i-CMC surfaces. α, β and γ are given by:

$$\alpha = 0 \ ; \ \gamma = P(0) \ ; \ \beta = \frac{P(h) - \gamma}{h}$$

Where h is an arbitrary length, taken for example as the average edge length of the 1-star boundary. Then:

$$z = -\gamma/\beta$$

Case $b \neq 0$

In that case, the equation is quadratic. We calculate coefficients α, β and γ as follows:

$$\gamma = P(0) \ ; \ \beta = \frac{P(h) - P(-h)}{2h} \ ; \ \alpha = \frac{P(h) - \beta h - \gamma}{h^2}$$

We then compute the discriminant $\Delta = \beta^2 - 4\alpha\gamma$. We choose the height z as follows:

- If $\Delta > 0$: For a type I solution, we choose the root solution $z = \frac{-\beta - \sqrt{\Delta}}{2a}$; for a type II solution, we choose $z = \frac{-\beta + \sqrt{\Delta}}{2a}$
- If $\Delta = 0$, we obviously return the only solution;
- If $\Delta < 0$, we output the critical point, which minimizes $|aH + bK - c|$:

$$z = -\frac{\beta}{2\alpha}$$

4.5 Validation

The generation method is validated using again paraboloids. By generating a surface with the analytical boundaries of a paraboloid, one can obtain an i-liwein mesh very close to the paraboloid. Examples are given in Figure 11. Curvatures, Gaussian and mean, both converge well to their expected value. Results are given for 1000 iterations

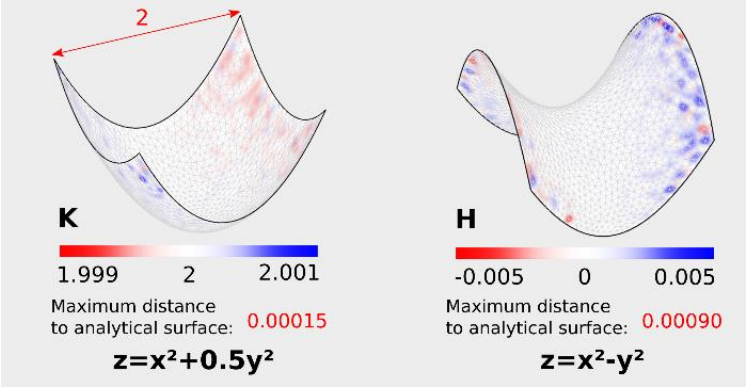

Figure 11: Validation of generation method - Construction of paraboloids from their boundaries as i-liwein surfaces

Note:

To finish our discussion about vertex-wise approximation of curvatures, related to (Borrelli et al. 2003), we remark that that the discrete scheme of K^i and H^i, which were giving poor results for a mesh *inscribed* in an i-liwein surface, can actually converge very well to the smooth curvatures of the underlying surface (whatever the vertex valence) if the mesh approximates the surface without being inscribed in it, i.e. if its vertices are not constrained to be on the surface.

4.6 Cases of non-existence of solutions

We do not have theoretical results on the convergence of our method. For convex boundaries (i.e. boundaries for which the projection in the xy plane defines a convex domain of the plane), existence of solutions to our form of the Monge-Ampere is guaranteed, and our method proves to be fairly robust. However, there is at the moment no existence result regarding non-convex boundaries. Practically, instability may be encountered on non-convex boundaries: if parameter b is pushed to a certain value, and if $|c|$ is low, then the vertex height may diverge. This may happen even at low values of b if the domain has holes with a highly curved concave boundary. The search of existence of solutions for non-convex boundaries for given parameters (a, b, c) is beyond the scope of this paper.

5 Designing with i-liwein surfaces

The generation algorithm presented in section 4 and the analytical primitives shown in section 2 may be used to design various typologies of structures which simultaneously have planar panels and are funicular or self-stressed.

5.1 Membranes and cable nets

With $c = 0$, surfaces $aH^i + bK^i = 0$ correspond to the equilibrium shapes of self-stressed membranes or cable nets. The shape of i-liwein membranes can be understood by comparing i-minimal with minimal surfaces. Minimal surfaces correspond to shapes of soap films, they have

been a great source of inspiration for the design of textile membranes in architecture (Bach, Burkhard, and Otto 1988). Compared with minimal surfaces, i-minimal surfaces:

- Cannot be self-stressed with constant isotropic membrane stresses. They still correspond to self-stressed membranes (proposition 1), but the constant isotropic quantity is their projected stresses. This implies that membrane stresses are higher in areas of high slope;
- Are restricted to shapes that are field heights;
- Can join boundaries with significant height difference, which cannot be interpolated by a single minimal surface.

The shape differences are illustrated in Figure 12. i-minimal and minimal surfaces are created on the same three boundaries, with increasing height differences between the large oval on the ground and the two loops at the centre. In the top row, the height difference is quite low, such that the difference between the two surfaces is hardly noticeable. In the middle row, the height difference is increased: the difference between the two surfaces is clear. Necking is observed in the minimal surface around the center loops, but not for the i-minimal surface, which is actually just a scaled copy (in the z-direction) of the one above. In the bottom row, the height difference is further increased. There does not exist anymore a stable minimal surface fitting the boundary curves.

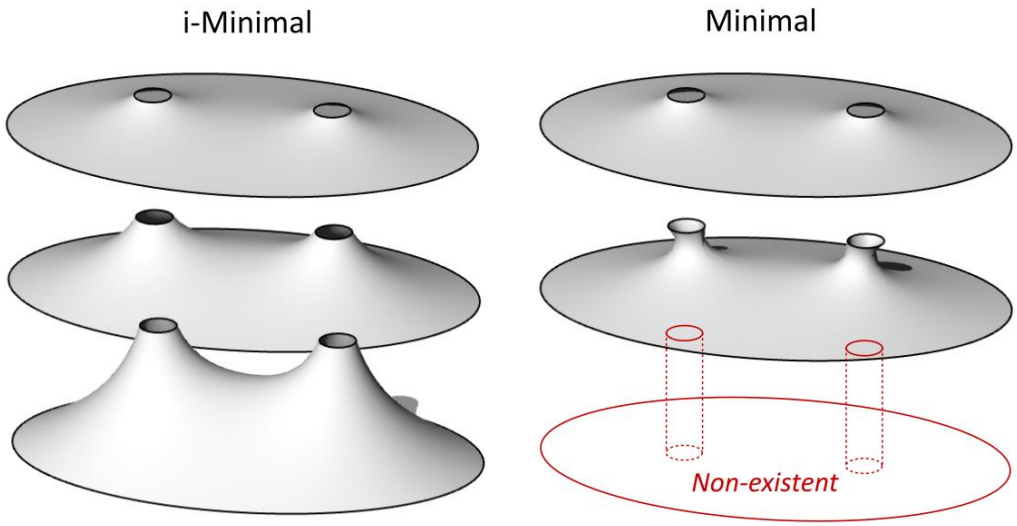

Figure 12: Comparison of the shape of i-minimal and minimal membranes on three sets of boundary curves, with increasing height difference.

i-liwein membranes do not require that the isotropic direction is vertical: whatever the direction, they correspond to a self-stressed membrane geometry. Therefore, on a given boundary, the isotropic direction can be tilted to explore shape variations. An example is shown in Figure 13, where three i-minimal surfaces are generated on the same boundaries (two coaxial circles), but

with different isotropic directions (indicated by red arrows). In each case, the stresses projected in the plane perpendicular to the red arrows are constant.

Figure 13: i-minimal membranes constructed on the same boundary, but with different isotropic directions

The effect of parameter b on the geometry can be visualised in Figure 2. It makes the surface tend towards the upper or lower portion of the convex envelope of the boundary curves.

Figure 14 shows Pelikan surfaces obtained by scaling the boundary in the x or y direction of an i-minimal surface (middle), creating an i-minimal surface on it, and scaling everything back to the original boundary. This result in with increased transverse (left figure) and longitudinal (right) tension.

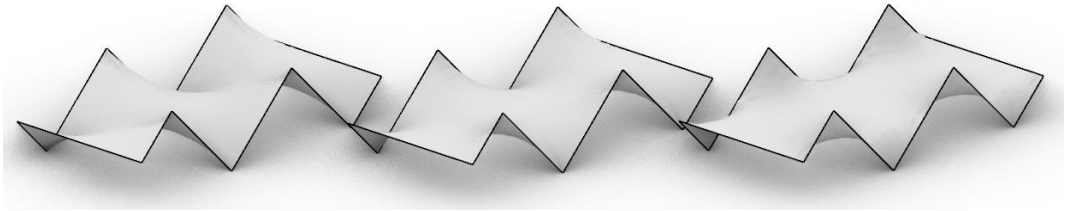

Figure 14: Middle: i-Minimal surface. Left and right: Pelikan surfaces with respectively increased transverse and longitudinal tension

Figures 12 to 14 illustrate how i-liwein surfaces may be used to design membranes. They were generated from the workflow of section 4. Figure 14 shows a cable net designed from a monkey saddle (such as the one shown in Figure 7). The pattern and the surface were derived from the analytical equation (given in 2.3.3).

5.2 Gridshells

For a gridshell, i-principal curvature directions of i-liwein surfaces combine both fabrication and mechanical properties. An application is illustrated in Figure 1 and Figure 15. An i-liwein surface is generated on a boundary composed of closed boundary curves – the boundary of Figure 15 mimics the one of the Chadstone gridshell. An i-principal curvature net is computed, and is used to define the position and orientation of the beams of a gridshell. Since the i-principal net forms a conjugate curve network, mesh faces are almost planar (an optimization could make them exactly planar with small vertex displacements). Furthermore, beams are aligned with principal stress directions under uniform vertical pressure (snow load), so they have a relevant orientation. Finally, we can notice that pattern drawn by i-curvature lines is smooth, and gives faces with approximately uniform size.

If one were to search by optimization of vertex positions the geometry of a gridshell combining planar quads and beams aligned with principal stresses, a main question would be: what is the right mesh combinatorics to start with? In i-liwein surfaces, this combinatorics appears naturally from the curvature field.

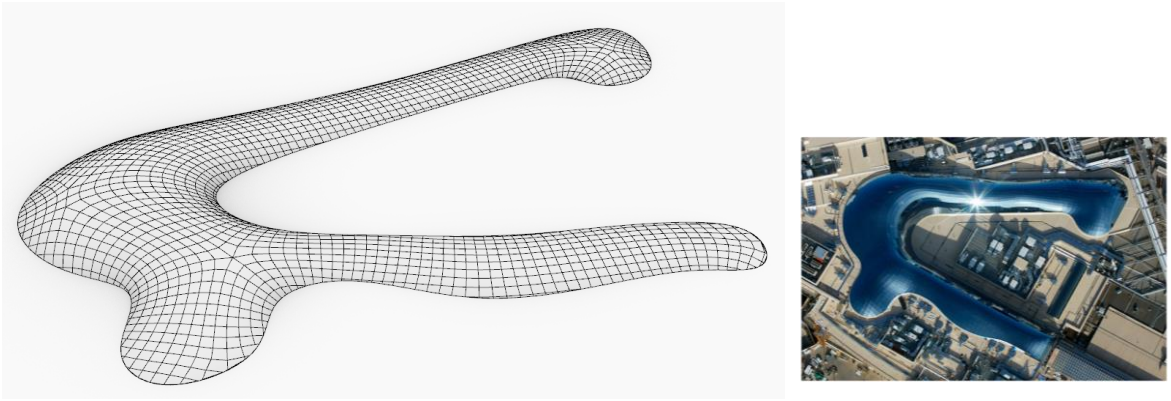

Figure 15: Funicular gridshell with planar quads, constructed by discretizing an i-CMC surface along i-principal curvature directions on the boundary of the Chadstone gridshell (right picture ©Seele)

5.3 Funicular shells

i-liwein surfaces can also be used to design funicular shells. The method allows a quick exploration of a 2-parameter family of funicular surfaces fitting a target boundary. For a concrete shell, the fact that i-principal curvature lines form a conjugate net could be used to simplify the fabrication of formwork. For example, the surface can be covered with developable strips so that thin flexible panels can be used as formwork.

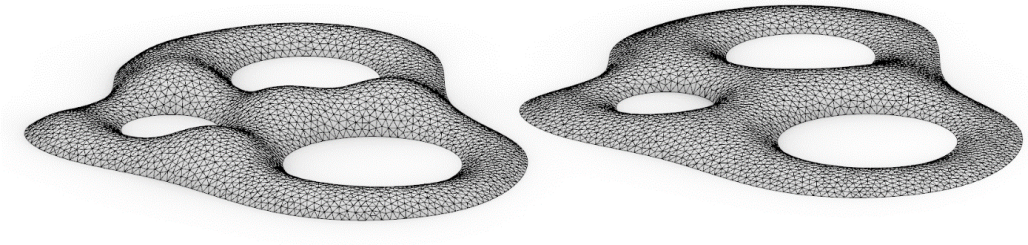

Figure 16: i-LW surfaces generated on the same boundaries as the gridshell of Figure 15.
Left: b>0. Right: b<0, close to the limit $a^2+4bc=0$ (this is a close-up of Figure 1)

The effect of parameters *b* and *c* on the surface geometry are the following: Parameter *c* allows to more or less inflate the surface (with a pressure acting vertically), while parameter *b* allows the control of the height difference between saddles and hill tops. This is illustrated in Figure 16, in which the reference surface of Figure 15 (which is i-CMC) is deformed. The left picture shows the case $b<0$: the surface looks like domes connected by low corridors. The right picture shows the case $b>0$: the surface now looks level, a more unified space is defined underneath.

6 Mechanical behavior: two case studies

In this section, we perform two case studies to investigate first the effect of parameters *a*, *b* and *c* on the mechanical behavior of a concrete shell, then the efficiency of i-curvature lines for defining the layout of a gridshell structure.

6.1 Application to concrete shell rooves

We compare three i-liwein surfaces (Figure 17) with the same boundary (that resembles an eight or a peanut), and same area (430m²), but different values of *b*. The constant area is ensured by adjusting the value of *c* while *b* varies (see table 1). With *b*<0, the height difference between the two domes and the valley is higher, while with *b*>0, the crest line is more uniform (see figure 15 and table 1). All three surfaces present two portions with positive Gaussian curvature on the side (the domes) and one portion with negative Gaussian curvature in the middle (the valley). Practically, the reference mesh is the same triangulated mesh with 1852 faces for the three surfaces.

Table 1: Geometric characteristics of the three i-liwein surfaces

a=0.5	C	Min Height of saddle	Max Height of dome	Max Gaussian curvature	Min Gaussian curvature	% flat area (|K| < 0.0016)
b=0 (iCMC)	0.083	1.51	2.54	-15.2	6.6	11.5%
b=1.7	0.076	1.13	2.61	-16.4	5.7	9.8%
b=-1.4	0.086	1.79	2.46	-15.0	7.8	14.7%

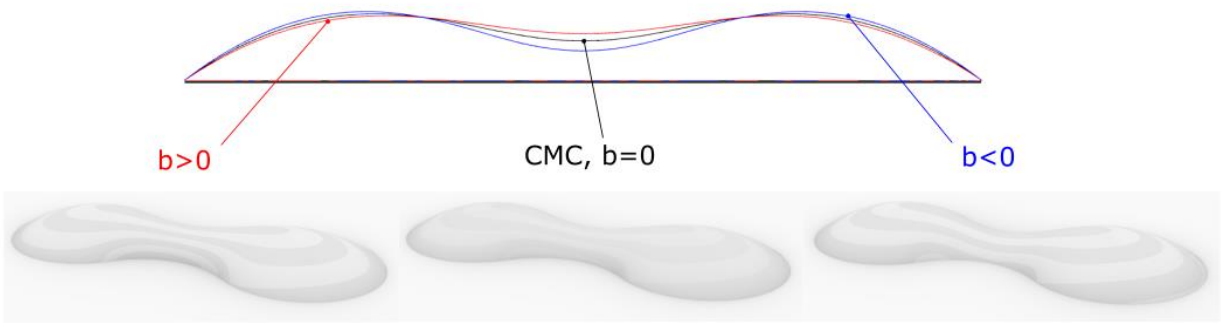

Figure 17: Influence of parameter *b* on the shape of i-liwein surfaces with same boundary curve and same area. Top: Longitudinal cut on the three shapes. Bottom: Perspective view (left: *b=1.4*, middle: *b=0* iCMC and right: *b=-1.7*).

Supposing now that these three surfaces are compared in terms of mechanical performances in order to build a concrete shell roof. The rise over span ratio of the surfaces remaining between

1/7 and 1/5, the shells cannot be considered as low shells and their behaviour should be similar and dominated by membrane actions with limited bending stresses. The thickness of the shell is uniform and equal to 10cm, so approximately 1/100 of the average span (10.5m). As the area is constant over the three surfaces, the quantity of material used for the three shells is the same. Differences in the structural response will thus be uniquely related to the shape of the shell.

Two support conditions are investigated: i) membrane supports with zero displacements in the tangent plane and ii) fixed supports with no translations and no rotations along the edge. The first one corresponds to the theoretical membrane model where the shell develop forces only within the surface. The second one corresponds to more practical concrete shell roof boundary conditions and will develop bending moments around the edge.

Two loading conditions are then applied to the shell: i) uniform vertical load on the whole structure, ii) uniform vertical load on one fourth of the structure. The shells are all funicular for the first load and should resist without bending, while they should exhibit some under the second load.

Two kinds of analysis are conducted: i) standard static linear analysis and ii) linear buckling analysis. The first one is used to retrieve principal stress pattern, as well as displacement measures; the second one critical buckling loads. Key information for comparison is not absolute but relative, the intensity of load and Young modulus being somewhat arbitrary (here 25kN/m² and 31GPa respectively). All calculations are conducted with finite element software Karamba3D.

Alignment of i-principal stresses with i-principal curvatures

For the three surfaces, one first compares the layout of i-principal stresses under uniform vertical load with i-principal curvature lines. The formers are calculated by simple integration of the membrane stress field in the shell by Karamba3d, the later from the principal curvature lines obtained by EvoluteTools Tmap. Both networks are calculated on a scaled down geometry by a factor of 10 in the z-direction so that principal network and i-principal network can be assimilated. As one can see on figure 16 for the iCMC surface on membrane supports, i-principal stresses and i-principal curvature coincide very well: the surface is hence funicular in the sense of isotropic geometry.

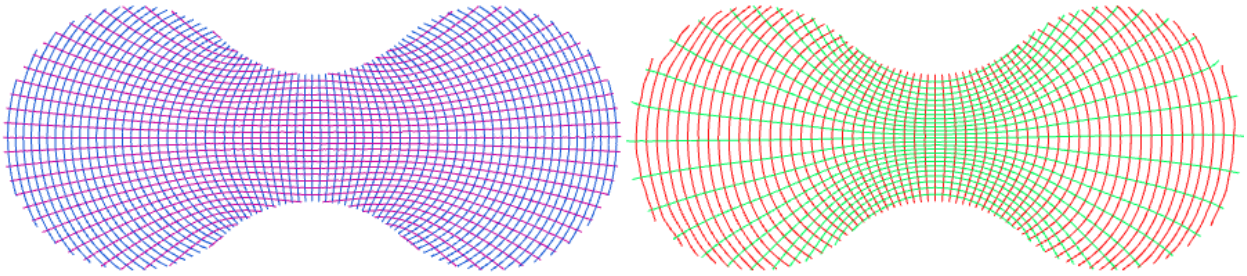

Figure 16: Comparison of i-curvature lines (left) and i-stress line (right) for an iCMC surface under UPL.

The alignment was tested for fixed boundary conditions and, as expected, the perturbations induced by the boundaries affect mainly the neighbourhood of the boundary. It remains very good in the central part of shell.

Buckling capacity

Concerning mechanical performances, several criteria were tested: maximum displacement, strain energy and buckling capacity which all lead to the same conclusions regarding the influence of the shell shape. For conciseness, it was thus chosen to focus on the buckling capacity which is often the sizing criterion for concrete shell structures. Critical factors for the three surfaces under both loadings with both boundary conditions have been reported in Table 2. One remarks that, for all cases, the capacity of the three shells compares well. Indeed, relative differences (max – min)/average range from 10% to 27% with membrane supports and fall down to a range of 4% to 6% with fixed edges. One can thus conclude that the shape has less influence than the boundary conditions. Once appropriated boundary conditions are given to the shell (here fixed supports), then the shape of the i-liwein shell has few influence on the capacity. This is true for the funicular load as well as for the non-symmetric loading on one quarter of the structure.

Table 2: Geometric characteristics of the three surfaces

supports	Loaded area	b=0	b=1.7	b=-1.4	Max-min/aver.
Membrane supports	Whole	317	288	300	10%
	quarter	324	252	335	27%
Fixed supports	Whole	477	448	464	6%
	quarter	568	552	547	4%

This small example demonstrates that the framework of i-liwein surfaces provides to the designer a whole family of shapes with constant area (and by there, constant volume of material) and similar mechanical performances. This family of shapes can be explored easily with help of two

parameters, *b* and *c* (which are not independent if the area has to remain constant) in order to satisfy other criteria than mechanical performance, such as aesthetic or functionality.

6.2 Application to steel gridshell structures

The interest of i-liwein surfaces for structural engineers is further investigated through a gridshell variant of the iCMC surface studied in previous section. To obtain the grid layout, the following procedure was applied:

Form the desired surface by adjusting parameters *b* and *c* for a given boundary;

Scale down the surface and find the network of principal curvatures;

Project this network vertically on the surface.

Build the gridshell on this network orienting cross-section according the bisecting plane of adjacent faces.

The generated grids have by construction quasi-flat quadrangular panels because they follow a conjugate network on the reference smooth surfaces. In the present case (the iCMC surface studied in previous section), the maximum out-of plane default (calculated as the distance between quad diagonals relatively to the length of the largest diagonal) is hence below 1%. It can be easily reduced by a short optimisation for planarity of the node positions. Indeed, authorising a displacement of maximum 2cm around the initial position on the mesh allow to fit standard construction tolerances for glass panels (i.e. out of plane default below 0.5%).

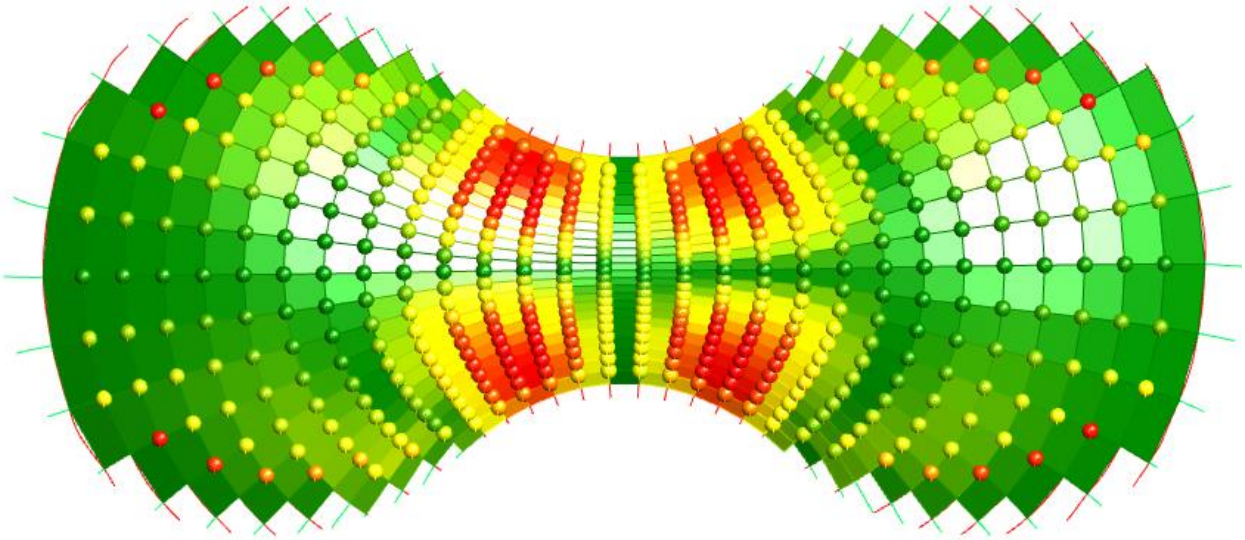

Figure 16: Planarity of quad panels (coloured quad from green 0% to red 0.5% out-of plane default) and torsion at node (coloured spheres from green 0 mrad to red 15 mrad angular torsion at nodes) of a gridshell built on i-curvature lines of an i-CMC surface.

Theoretically, non-trivial offsets with torsion free nodes are guaranteed on gridshells built on curvature lines, not on i-curvature lines. However, the geodesic torsion of i-curvature lines is still small and they can build some reasonable inputs for optimisation. In the present case after planarization of faces, no optimisation is computed but torsion at nodes is evaluated considering that the local beam planes are set according to the bisecting plane of adjacent panels (i.e. normal to the surface). One can hence build four axes at nodes by intersecting the beam planes and compute the angles between node axes which gives an estimation of torsion at nodes. Here the maximum is of 10 mrad, which corresponds to 1 mm for a 10 cm beam and is almost acceptable as it is.

Once the grid is found, it is tested for funicularity and submitted to a uniform projected load (UPL): each node is loaded according to its tributary area in the top view with 1kN/m². It is also loaded with the same load applied on one quarter of the surface. All connexions between members are fixed, as well as all supports on the ground. A rectangular hollow section of 100x50x8 is attributed to all members orienting the cross-section according to the bisecting plane of adjacent faces. Extremal values of internal forces are shown in table 3.

Table 3: Internal forces in the gridshell built on the i-curvature lines of the iCMC surface

	UPL		UPL on one quarter		ratio	
N [kN]	-11.5	0.02	-40.7	22	4	
M_t [kNm]	-0.012	0.012	-0.51	0.46	43	38
M_y [kNm]	-0.17	0.13	-4.7	4.1	27	30
M_z [kNm]	-0.03	0.04	-1.5	1.5	44	37

Under uniform projected load, the structure is hence under pure compression: no tension arises and the average bending stresses represent less than 1% of the total stresses. One can thus conclude that the gridshell is funicular of UPL, verifying hence the discrete version of the theorem demonstrated earlier for the smooth geometry. Under non symmetric loading (UPL on one quarter of the grid), bending forces are multiplied by 40 in the weak direction and torsion compared to UPL. These moments correspond to shear forces in the equivalent continuous membrane which were almost equal to zero under UPL because the beams are aligned with i-principal stress directions. In the strong axis, the increase is large but smaller because under UPL some bending moments were already induced by edge effects near the supports. However, stresses due to normal forces still represent 87% of the total stress in average (more than 80%

for 80% of beams) which demonstrates that this kind of funicular gridshell is also very efficient under non-symmetrical loads.

7 Discussion

Application to design and comparison with other methods

Our proposed framework has the following limitations. Firstly, although i-liwein surfaces are efficient for uniform vertical load, a final design would require checking asymmetrical loads and buckling. They might not be optimal then. Secondly, the proposed method does not give access to the entire design space of surfaces of funicular planar quads.

However, a strength of the proposed method is the speed at which a designer can explore a rich design space in a project. Compared to the popular "topology to shape" methods discussed in section 1.1, designers need not input trial topologies, a step which may by time consuming for complex boundaries. Even though this preliminary shape might not be the final one, the designer knows a shape that works, and can still deform it afterwards to account for other constraints.

Considering both strengths and limitations, we believe our method is particularly suited for conceptual design phases, especially in situations in which one wants to explore curved options such as gridshells or membranes with very limited available time.

Implementation details

The algorithm described and used in sections 4 and 5 was implemented by scripting the software Rhino/Grasshopper. All the numerical images of this section were generated from that script. The linear algebra package Math.net numerics is used to diagonalize curvature and stress matrices. The i-Principal net in Figure 1 or 14 are computed in three steps:

1. The surface is scaled down in z direction such that its height is significantly lower than its width. In this state, principal and i-principal directions nearly coincide.
2. A principal net is computed, using commercial software Evolute Tmap.
3. The net and the surface are scaled back in the z direction to fit the original geometry. We use the fact that i-principal directions are invariant under z scaling (the eigenvectors of $\nabla^2 f$ are the eigenvectors of $\lambda\nabla^2 f$ (with $\lambda \in \mathbb{R}$)).

In the current setup, a designer can interactively deform a surface by controlling parameters. It takes about 10 seconds to deform a mesh with 500 vertices to a near LW surface on a 3.5GHz CPU with 16Go of RAM, and get a good idea of the final shape. Full convergence (displacements

below 1/1000 of surface dimensions) takes about a minute, but could be made much faster by not displaying intermediate calculation steps and using a second order solver, like L-BFGS. In particular, we remark that if $b = 0$, our algorithm does not benefit from the linearity of the problem. Faster resolution methods are a topic of future work.

Elastic deformations

i-liwein surfaces admit an admissible membrane stress field under uniform vertical load. They hence correspond to equilibrium shapes of *deformed* configurations. However, there is no guaranty that an i-liwein will stay i-liwein under elastic deformation, or even that i-liwein surfaces can be obtained exactly by elastic deformation of an initially stress-free material configuration. The study of this problem could be addressed in future work. However, these are not issues in the considered applications:

- In the case of a funicular shell, displacements are very small. If the initial state is i-liwein, the deformed state will be nearly i-liwein. The analytical stress fields can then be used for limit analysis, for example for checking that a funicular surface can be found within the middle third of the cross section of a masonry shell (Heyman 1997). In the case of a concrete shell, the surface also does not need to be exactly i-liwein, as it can accommodate some bending.
- In the case of a tensile membrane, our approach is similar to popular methods such as force densities or dynamic relaxation method: Both methods also yield a deformed configuration at equilibrium. Potential incompatibilities are usually not a problem, because patterning and pretensioning is an approximate task anyway: tension is applied in warp and weft directions to membrane patches, so the actual deformed configuration is always a bit different from the target surface. In worst case, this leads to small waves on the surface.

Buckling

As stresses are known analytically, there might be ways to assess buckling loads under uniform load analytically. This could be the topic of future work.

Conclusion

This article showed the relevance of isotropic Linear Weingarten (“i-liwein”) for architectural design, with applications to many structural typologies: gridshells, membranes, shells and cable nets. It was proven that these surfaces remarkably combine mechanical and fabrication

properties: they may be covered by a pattern of planar quadrangles which is also funicular under a uniform load or self-stressed. A generation method based on discrete differential geometry was proposed. i-liwein surfaces appear to offer an interesting design space, with a control from boundary curves which is well suited for many architectural projects. Parameters a, b and c offer a global shape control, which is particularly interesting for editing complex shapes. The low amount of pre-processing required for the designer makes this method particularly suited in the context of conceptual design explorations.

On a final note, it is remarkable to observe how constant mean-curvature surfaces and Linear Weingarten surfaces are funicular for a normal pressure or a vertical pressure depending on the type of geometry used to define the curvature: Euclidian or isotropic.

Acknowledgement

We would like to warmly thank Pr. István Sajtos for bringing Pelikan surfaces to our attention, as it initiated this project on isotropic linear Weingarten surfaces. We would also like to warmly thank Laurent Monasse for fruitful discussions.

References

Adriaenssens, Sigrid, Laurent Ney, Eric Bodarwe, and Chris J. K. Williams. 2012. “Finding the Form of an Irregular Meshed Steel and Glass Shell Based on Construction Constraints.” *Journal of Architectural Engineering* 18(September):206–13.

Bach, Klaus, Berthold Burkhard, and Frei Otto. 1988. *IL18 Forming Bubbles*. Institute for Lightweight structures, University of Stuttgart.

Benamou, Jean-David, Brittany D. Froese, and Adam M. Oberman. 2014. “Numerical Solution of the Optimal Transportation Problem Using the Monge – Ampère Equation.” *Journal of Computational Physics* 260:107–26.

Benamou, Jean David, Brittany D. Froese, and Adam M. Oberman. 2010. “Two Numerical Methods for the Elliptic Monge-Ampère Equation.” *ESAIM: Mathematical Modelling and Numerical Analysis* 44(4):737–58.

Block, Philippe. 2009. “Thrust Network Analysis. Exploring Three-Dimensional Equilibrium.” PhD Thesis, MIT.

Bo, Pengbo, Helmut Pottmann, Martin Kilian, Wenping Wang, and Johannes Wallner. 2011. “Circular Arc Structures.” *ACM Trans. Graph.* 30(4):101:1–101:12.

Borrelli, Vincent, Frédéric Cazals, and Jean-Marie Morvan. 2003. “On the Angular Defect of Triangulations and the Pointwise Approximation of Curvatures.” *Computer Aided Geometric Design* 20(6):319–41.

do Carmo, Manfredo P. 1976. *Differential Geometry of Curves and Surfaces*. Prentice-Hall, Inc.

Cartan, Henri. 1963. *Elementary Theory of Analytic Functions of One or Several Complex Variables*. Editions s. Addison-Wesley Inc.

Courant, R., and D. Hilbert. 1962. *Methods of Mathematical Physics - Volume II - Partial Differential Equations*. Wiley-VCH Verlag.

Dean, Edward J., and Roland Glowinski. 2003. "Numerical Solution of the Two-Dimensional Elliptic Monge-Ampère Equation with Dirichlet Boundary Conditions: An Augmented Lagrangian Approach." *Comptes Rendus Mathematique* 336(9):779–84.

Dean, Edward J., and Roland Glowinski. 2004. "Numerical Solution of the Two-Dimensional Elliptic Monge-Ampère Equation with Dirichlet Boundary Conditions: A Least-Squares Approach." *Comptes Rendus Mathematique* 339(12):887–92.

Feng, Ruo Qiang, and Jin Ming Ge. 2013. "Shape Optimization Method of Free-Form Cable-Braced Grid Shells Based on the Translational Surfaces Technique." *International Journal of Steel Structures* 13(3):435–44.

Feng, Xiaobing, and Max Jensen. 2017. "Convergent Semi-Lagrangian Methods for the Monge–Ampere Equation on Unstructured Grids." *SIAM J. NUMER. ANAL* 55(2):691–712.

Frey, François, and Marc-André Studer. 2003. *Traité de Génie Civil, Volume 5 - Analyse Des Structures et Milieux Continus - Coques*. Presses polytechniques et universitaires romandes.

Glymph, James, Dennis Shelden, Cristiano Ceccato, Judith Mussel, and Hans Schober. 2004. "A Parametric Strategy for Freeform Glass Structures Using Quadrilateral Planar Facets." *Automation in Construction* 13(2):187–202.

Heyman, Jacques. 1997. *The Stone Skeleton: Structural Engineering of Masonry Architecture*. Cambridge University Press.

Hincz, Krisztián, and Zsolt Gaspar. 1999. "The Effect of the Apporximations Used during Generation of Membrane Cutting Pattern.Pdf." *Archives of Civil Engineering* 45(2):221–30.

Jensen, Max. 2018. "Numerical Solution Of The Simple Monge–Ampère Equation With Nonconvex Dirichlet Data On Nonconvex Domains." Pp. 129–42 in *Hamilton-Jacobi-Bellman Equations*. Walter de Gruyter GmbH,Berlin/Munich/Boston.

Mesnil, Romain, Cyril Douthe, Christiane Richter, and Olivier Baverel. 2018. "Fabrication-Aware Shape Parametrisation for the Structural Optimisation of Shell Structures." *Engineering Structures* 176(July):569–84.

Neilan, Michael, Abner J. Salgado, and Wujun Zhang. 2020. "The Monge–Ampère Equation." Pp. 105–219 in *Handbook of Numerical Analysis*.

Oberman, Adam M. 2008. "Wide Stencil Finite Difference Schemes for the Elliptic Monge-Ampère Equation and Functions of the Eigenvalues of the Hessian." *Discrete Contin. Dyn. Syst. Ser. B,* 10(1):221–38.

Ogrenmis, Alper Osman. 2016. "Rotational Surfaces in Isotropic Spaces Satisfiying Weingarten Conditions." *Open Physics* 14(1):221–25.

Oval, Robin. 2019. "Topology Finding of Patterns for Structural Design." PhD Thesis, Université Paris-Est, ETH Zürich.

Oval, Robin, Matthias Rippmann, Romain Mesnil, Tom Van Mele, Olivier Baverel, and Philippe Block. 2018. "Topology Finding of Structural Patterns." Pp. 342–63 in *Advances in Architectural Geometry*.

Pelikan, J. 1958. "Membrane Structures." in *Proc of the Second Symp. on Concrete Shell Roof Construction, Teknisk Ukeblan, Oslo*, edited by A.-J. A. and E. Al.

Pellis, Davide, and Helmut Pottmann. 2018. "Aligning Principal Stress and Curvature Directions." Pp. 34–53 in *Advances in Architectural Geometry*.

Pottmann, Helmut, and Yang Liu. 2007. "Discrete Surfaces in Isotropic Geometry." Pp. 341–63 in *IMA international conference on mathematics of surfaces*. Springer, Berlin, Heidelberg.

Ramm, Ekkehard, and W. A. Wall. 2004. “Shell Structures - A Sensitive Interrelation between Physics and Numerics.” *International Journal for Numerical Methods in Engineering* 60(1):381–427.

Sachs, Hans. 1990. *Isotrope Geometrie Des Raumes*. Friedr. Vi.

Sauer, R. 1970. *Differenzengeometrie*. Springer, Berlin.

Schiftner, Alexander, and Jonathan Balzer. 2010. “Statics-Sensitive Layout of Planar Quadrilateral Meshes.” Pp. 221–36 in *Advances in Architectural Geometry*.

Schling, Eike, Denis Hitrec, and Rainer Barthel. 2017. “Designing Grid Structures Using Asymptotic Curve Networks.” *Humanizing Digital Reality, Design Modelling Symposium, Paris*.

Sun, Xiang. 2016. “Discrete Curvature Theories and Applications.” Ph. D. thesis, King Abdullah University of Science and Technology, Thuwal.

Tang, Chengcheng, Xiang Sun, Alexandra Gomes, Johannes Wallner, and Helmut Pottmann. 2014. “Form-Finding with Polyhedral Meshes Made Simple.” *ACM Transactions on Graphics* 33(4).

Tellier, Xavier, Cyril Douthe, Laurent Hauswirth, and Olivier Baverel. 2019a. “Linear Weingarten Surfaces for Conceptual Design.” in *Proceedings of the International fib Symposium on Conceptual Design of Structures*.

Tellier, Xavier, Cyril Douthe, Laurent Hauswirth, and Olivier Baverel. 2019b. “Surfaces with Planar Curvature Lines: Discretization, Generation and Application to the Rationalization of Curved Architectural Envelopes.” *Automation in Construction* 106.

Tellier, Xavier, Cyril Douthe, Laurent Hauswirth, and Olivier Baverel. 2020. “Linear-Weingarten Membranes with Funicular Boundaries.” *Structural Concrete* 1–14.

Tellier, Xavier, Cyril Douthe, Laurent Hauswirth, and Olivier Baverel. 2021. “Funicularity of Conics.” *Acta Mechanica* 232(8):3179–91.

Tellier, Xavier, Laurent Hauswirth, Cyril Douthe, and Olivier Baverel. 2018. “Discrete CMC Surfaces for Doubly-Curved Building Envelopes.” Pp. 166–93 in *Advances in Architectural Geometry*.

Trudinger, Neil S., and Xu-jia Wang. 2008. “The Monge-Ampère Equation and Its Geometric Applications.” *Handbook of Geometric Analysis, International Press* I:467–524.

Ventsel, Eduard, and Theodor Krauthammer. 2001. *Thin Plates and Shells. Theory, Analysis and Applications*. Vol. 66. Marcel Dekker.

Villani, Cédric. 2003. *Topics in Optimal Transportation*. American Mathematical Society. Graduate Studies in Matehmatics, Vol 58.

Vouga, Etienne, H. Mathias, Johannes Wallner, and Helmut Pottmann. 2012. “Design of Self-Supporting Surfaces.” *ACM Trans. Graph.* 31(4).

Wang, Wenping, and Yang Liu. 2009. “A Note on Planar Hexagonal Meshes.” Pp. 221–33 in *Nonlinear Computational Geometry*.

Wu, Rengmao, Liang Xu, Peng Liu, Yaqin Zhang, Zhenrong Zheng, Haifeng Li, and Xu Liu. 2013. “Freeform Illumination Design : A Nonlinear Boundary Problem for the Elliptic Monge – Ampére Equation.” *Optics Letters* January:229–31.

www.keramion.de. n.d. “Foundation KERAMION, Centre of Modern and Historical Ceramics in Frechen.” Retrieved December 10, 2019 (http://www.keramion.de/).

Yoon, Dae Won, and Jae Won Lee. 2016. “Linear Weingarten Helicoidal Surfaces in Isotropic Space.” *Symmetry* 8(11):1–7.

Zadravec, Mirko, Alexander Schiftner, and Johannes Wallner. 2010. “Designing Quad-Dominant Meshes with Planar Faces.” Pp. 1671–79 in *Computer Graphics Forum*. Vol. 29. Oxford, UK: Blackwell Publishing Ltd.